

PAPER



Cite this: *Catal. Sci. Technol.*, 2015, 5, 1961

Promotion effect of Fe in mordenite zeolite on carbonylation of dimethyl ether to methyl acetate†

Hui Zhou,^{abc} Wenliang Zhu,^{ab} Lei Shi,^{ab} Hongchao Liu,^{ab} Shiping Liu,^{abc} Shutao Xu,^{ab} Youming Ni,^{ab} Yong Liu,^{ab} Lina Li^{abc} and Zhongmin Liu^{*ab}

A series of Fe-modified mordenite zeolite samples were synthesized by a template-free method and employed in dimethyl ether (DME) carbonylation reaction for the production of methyl acetate (MAc). XRD, UV-Vis, and UV-Raman characterization studies proved that Fe atoms have been introduced into the mordenite zeolite framework by partial substitution of Al atoms, which led to evident changes of activity and MAc selectivity. With the increase of iron content (as metal) from 0.0 to 3.6 wt%, DME conversion first increased and then decreased. MAc selectivity and catalyst stability were enhanced for all Fe-modified samples. TG and GC-MS analysis of deactivated catalysts showed that the amount of coke retained in the catalysts decreased as the iron content of the zeolites increased. The enhancement effects were expounded in terms of the decrease of the acid strength and acid density in the 12MR channels of mordenite after introduction of Fe, resulting in the reduction of carbon deposition.

Received 1st December 2014,
Accepted 6th January 2015

DOI: 10.1039/c4cy01580k

www.rsc.org/catalysis

1. Introduction

The carbonylation reaction of dimethyl ether (DME) to methyl acetate (MAc) has triggered wide research interest^{1–8} because the product of MAc hydrogenation, ethanol, can be applied in wide fields.^{9–13} This novel production process of ethanol is highly competitive compared with the traditional processes of hydration of ethylene and fermentation of sugars and corns because DME can be readily derived from synthesis gas (CO + H₂, syngas).¹⁴ The copper-based catalyst for the hydrogenation reaction has been used in commercial operations. The major challenge in research on this novel process is developing effective heterogeneous zeolite catalysts for DME carbonylation reaction with excellent performance in terms of activity, selectivity and stability.

In 1984, Fujimoto *et al.* first reported results from studies of vapor carbonylation of methanol with heterogeneous zeolite catalysts. They found that HY and HMOR zeolite catalysts demonstrated some carbonylation activity with low MAc selectivity.¹ Iglesia and his co-workers^{2–4} initiated detailed

studies on DME carbonylation to MAc with zeolite catalysts (H-MOR, H-FER and H-ZSM5) and reported that the HMOR zeolite could catalyze DME carbonylation reaction to MAc at low temperatures (423–463 K) with remarkable selectivity (>99% MAc selectivity), but the MAc productivity was below the expected commercial target. Also, the HMOR catalyst with 8MR and 12MR channels had the highest MAc synthesis rate and the controlling step of carbonylation reaction (3) occurred in the 8MR channels. Quantum chemical calculation results⁵ showed that only the T3-O33 positions in the 8MR channels of mordenite were selective for acetyl generation. The highly selective properties of the HMOR catalyst was not only due to the size of 8MR channels but also to the unusual orientation of the methoxy group with respect to the 8MR channel (parallel to the cylinder axis).⁵ The *in situ* solid-state NMR spectroscopy studies also confirmed that the important surface acetyl intermediate species could only be identified in the 8MR channels, not in the active sites in the 12MR channels which favor the formation of hydrocarbons.⁶ According to the present understanding of this reaction, catalyst stability, one of the important factors for industrial application, can be enhanced through the occupation or removal of the acid sites in the 12MR channels of mordenite, where the formation of high molecular weight hydrocarbons like aromatics occurs, resulting in the deactivation of catalysts. Shen *et al.* reported the related study on the development of improved zeolite catalysts for DME carbonylation by pre-adsorption of pyridine⁷ or selective dealumination of the H-mordenite zeolite,⁸ obtaining

^a National Engineering Laboratory for Methanol to Olefins, Dalian Institute of Chemical Physics, Chinese Academy of Sciences, P. O. Box 110, 116023 Dalian, PR China. E-mail: liuzm@dicp.ac.cn; Fax: +86 0411 84379518; Tel: +86 0411 84379518

^b Dalian National Laboratory for Clean Energy, Dalian Institute of Chemical Physics, Chinese Academy of Sciences, Dalian, PR China

^c Graduate University of Chinese Academy of Sciences, Beijing 100049, PR China

† Electronic supplementary information (ESI) available. See DOI: 10.1039/c4cy01580k

considerable improvement in the performance of MOR catalysts for DME carbonylation reaction.

Introduction of metal atoms in the framework or extra-framework of zeolites is an important route for changing the physiochemical properties of zeolites and thus improving their performance in reactions.¹⁵ Brian Ellis *et al.* reported that H-MOR and Cu-MOR were active and selective for methanol vapor phase carbonylation reaction under moderate operating conditions.¹⁶ For DME carbonylation reaction, introduction of Cu and Ag by ion exchange to replace H counterions was reported in publications and patents.^{17,18} FTIR and solid state NMR studies proved that Cu-H-MOR have two neighboring sites, bridged hydroxyl and neighboring Cu⁺, and contributed to the formation of MAc. Besides the activity, the product selectivity and stability of catalysts are major challenges in the development of DME carbonylation reaction. Zeolites containing Fe in their frameworks showed excellent performance in many catalytic reactions.^{19,20} Here, we report the results from studies of DME carbonylation with Fe-modified mordenites which were synthesized by a template-free hydrothermal method. The physical structure of the Fe³⁺ framework-substituted mordenites was characterized by XRD, UV-Vis, UV-Raman and N₂-adsorption and the acid site strength and density were characterized by ³¹P MAS NMR and FTIR spectroscopy after the adsorption of base probe molecules.

2. Experimental

2.1 Catalyst preparation

Iron nitrate [Fe(NO₃)₃·9H₂O], sodium aluminate [NaAlO₂], and silica sol (30% Si content) were used as initial Fe, Al, and Si sources, respectively. Si/Al in sol was 10 and the desired Fe contents were 0.0 wt%, 0.9 wt%, and 1.8 wt%, 3.6 wt% in the proposed product Na_(x+y)Fe_xAl_ySi₂O_{2(x+y+z)}, estimated by the formula:

$$\text{Fe}_{\text{wt}\%} = \frac{\text{Fe}_{\text{wt}}}{\text{Fe}_{\text{wt}} + \text{Al}_{\text{wt}} + \text{O}_{\text{wt}} + \text{Si}_{\text{wt}} + \text{Na}_{\text{wt}}} \times 100\%$$

The gel was sealed in a Teflon beaker and heated at 453 K with agitation. After crystallization for 20 h, the solid product was filtered and washed with deionized water. The products were labeled as FeNaMOR-0, FeNaMOR-0.9, FeNaMOR-1.8 and FeNaMOR-3.6. HMOR samples were obtained from NaMOR samples by ion exchange. The NaMOR sample was dispersed in NH₄NO₃ aqueous solution (1 mol L⁻¹, 1 g of the solid in 10 mL of the solution) at 353 K for 2 h and then filtered and washed with deionized water. After repeating ion exchange three times, the resulting solid was dried at 393 K overnight in ambient air and then calcined in flowing dry air (20 mL min⁻¹ g⁻¹) at 673 K for 8 h. The as-prepared catalysts were labeled FeHMOR-0, FeHMOR-0.9, FeHMOR-1.8 and FeHMOR-3.6.

2.2. Catalyst characterization

X-Ray powder diffractograms were recorded at room temperature using Cu K α radiation (PANalytical X'Pert Pro diffractometer).

The iron content was determined by XRF analysis (PANalytical AXIOS).

UV-Vis reflectance spectra were collected on a Varian Cary spectrophotometer from powdered Fe-containing samples with BaSO₄ used as a reference.

IR spectra in the framework vibration region were recorded with a spectral resolution of 4 cm⁻¹ using the KBr technique (weight ratio of the sample to KBr, 1:100).

UV-Raman spectra were recorded on a DL-2 Raman spectrometer, with a collection time of 300 s. A 244 nm line of a LEXEL laser was used as the excitation source. The laser power on the sample was less than 5 mW. The spectrometer used for Raman scattering was an Acton triple monochromator. A Princeton CCD detector was used to collect the spectra.

Nitrogen sorption experiments were performed at 77 K on a Micromeritics ASAP-2020 system in static measurement mode. The tested samples were degassed at 623 K for 4 h prior to each measurement. BET surface areas were calculated by the standard multi-point method, and the pore volume was determined by N₂ adsorption at a relative pressure of 0.98.

The ³¹P MAS NMR spectra were recorded on a Bruker Avance III 600 spectrometer using a 4 mm probe. The ³¹P MAS NMR spectra were acquired with high-power decoupling, a repetition time of 4 s, a $\pi/4$ pulse length of 2 μ s and a spinning speed of 12 kHz. The ³¹P NMR chemical shifts were referenced to 85% H₃PO₄. In a typical adsorption experiment, the FeHMOR zeolite was subjected to dehydration before adsorption of trimethylphosphine oxide (TMPO) probe molecules. The temperature of the sample increased to 673 K at a rate of 2 K min⁻¹ and maintained for 8 h and then cooled to room temperature. After the TMPO dissolved in CH₂Cl₂ was added to the sample in a three-neck round-bottomed flask in a N₂ glovebox, the sample was stirred overnight in the N₂ atmosphere. The removal of CH₂Cl₂ was conducted at about 323 K. The sealed sample vessel was further subjected to baking treatment at 453 K for 8 h to ensure the uniform adsorption of TMPO on the channels of mordenite. Then the TMPO crystals that did not react with the sample were evacuated at 453 K.

Fourier transform infrared (FT-IR) spectra after pyridine adsorption were obtained on a Bruker Tensor 27 instrument with a resolution of 4 cm⁻¹. Samples were pressed into a self-supporting wafer ($R = 0.65$ cm, 15 mg) and evacuated (2×10^{-2} Pa) in an IR cell at 673 K for 1 h prior to each measurement. Adsorption of pyridine was conducted at 573 K for 15 min to ensure saturated loading and then evacuation was carried out for 1 h prior to acquisition of IR spectra. The densities of Brønsted and Lewis acid sites were calculated from the IA values of the difference spectra at 1540 and 1450 cm⁻¹, respectively, using the extinction coefficients reported by Emeis.²¹

Thermal gravimetric (TG) analysis of deactivated catalysts was conducted on an SDT-Q600 instrument (TA, USA). In a typical TG experiment, about 20 mg of the sample was pre-treated with N₂ (100 mL min⁻¹) at 473 K for 1 h to remove the adsorbed moisture from the catalyst sample. After cooling to

room temperature in N₂, the sample was heated to 1073 K in an air flow (100 mL min⁻¹) at a heating rate of 10 K min⁻¹.

Organic species trapped in the channels of the mordenite zeolites during reactions were analyzed following the procedures as described in the literature.²² Spent catalysts were dissolved in 20% hydrofluoric acid solution. The organic phase was extracted with dichloromethane (CH₂Cl₂) and then analyzed using an Agilent 7890A/5975C GC/MSD.

2.3. Catalytic tests

DME carbonylation experiments were performed in a continuous flow fixed-bed stainless steel reactor. 1.0 g of the catalyst (40–60 mesh) was packed in the reactor and pretreated in N₂ at 673 K for 2 h. After cooling the catalyst sample to 473 K, a reactant gas mixture (5% DME, 35% CO, and 60% H₂) was introduced into the reactor at a gas hourly space velocity (GHSV) of 1500 mL (g h⁻¹). The reaction pressure was 3.0 MPa. The outlet gas was analyzed online using a gas chromatograph (Agilent 7890A) equipped with TCD and FID detectors.

3. Results and discussion

3.1. Structure analysis

The XRD patterns of Fe-modified HMOR samples with various iron contents are shown in Fig. 1 and Table 1. The typical diffraction peaks of mordenite-type zeolites are clearly observed for the four samples without any other crystalline diffraction peaks. As shown in the diffraction patterns in Fig. S1,† it is obvious that the peaks shift to the lower frequencies with the increase of iron content, indicating the increase of *d* values, the basal spacing. This is the prominent proof that the larger Fe³⁺ (0.63 Å) was introduced in the mordenite framework, replacing the smaller Al³⁺ (0.53 Å).²³ The relative crystallinities of the samples were calculated according to the sum of the areas of the seven strong peaks between 2θ of 5 and 30°, assuming that the relative crystallinity of the FeHMOR-0 zeolite was 100%. The comparison of the 96% and 104% relative crystallinities of FeHMOR-0.9 and FeHMOR-1.8 with the 100% relative crystallinity of

Table 1 Relative crystallinities and iron content of the FeHMOR samples

	Relative crystallinity	Si/(Al + Fe) (XRF)	Iron content, wt% (XRF)
FeHMOR-0	100%	7.5	0.04
FeHMOR-0.9	96%	7.2	0.89
FeHMOR-1.8	104%	7.1	1.62
FeHMOR-3.6	56%	6.6	3.05

FeHMOR-0 indicated that the two samples exhibit a good crystal state after the introduction of iron but the 56% relative crystallinity of FeHMOR-3.6 showed that the framework of mordenite collapsed to some extent as the iron content increased from 0 to 3.6%. As summarized in Table 1, the iron element content measured by XRF is about 0.04, 0.89, 1.62 and 3.05 wt% respectively and is in accordance with the designed contents.

The substitution of Fe for Al and the increased iron content resulted in the progressive loss of the IR framework bands' sharpness and shifting of the bands to lower wavenumbers, as shown in Fig. S2.† The band most sensitive to the substitution is the internal asymmetric stretching vibration of Si–O–T observed at 1084 cm⁻¹ for aluminosilicate.²³ The differences in terms of this band between the four samples indicated that Fe was already in the framework of the Fe-modified HMOR samples.²³ The information in Fig. S2† is consistent with the results of XRD presented above and further confirms the existence of Fe in the framework of the mordenites.

Fig. S3† shows the UV-Vis reflectance spectra measured for FeNaMOR samples containing different contents of iron at room temperature. Two common features are observed in the spectra of the Fe-modified mordenites: the strong absorption bands in the 200–300 nm interval due to charge transfer from the ligand to isolated framework Fe³⁺ ions, and the weak bands in the range of 370–450 nm related to the d–d transitions of Fe³⁺ ions with a tetrahedral symmetry.^{23–26} Therefore, Fe in the modified Na-mordenites was dominated by tetrahedral Fe³⁺ ions.

UV resonance Raman spectroscopy is a unique, practical and powerful technique for the detection of isolated transition metal atoms in the frameworks of zeolites.^{27–29} The laser line at 244 nm was used as the excitation source because it was close to the charge transfer bands at 230 nm. In the resonance Raman spectra of the transition metal substituted zeolites, the observed bands at about 500 and 1100 cm⁻¹ could be taken as the characteristic bands for the presence of transition metal ions in tetrahedral coordination in the framework sites of the zeolites.²⁸

The UV resonance Raman spectra of the FeHMOR samples with various iron contents excited by the 244 nm excitation line are shown in Fig. 2. The bands centered at about 400, 450, 800 cm⁻¹ are the characteristic bands of the MOR structure.³⁰ The bands at 520 and 1050 cm⁻¹ are the resonance Raman bands associated with the isolated iron species in the framework due to the Fe–O–Si symmetric and asymmetric stretching modes of the isolated tetrahedral iron ions in the silica framework, respectively.^{28,31} As in the report on the UV

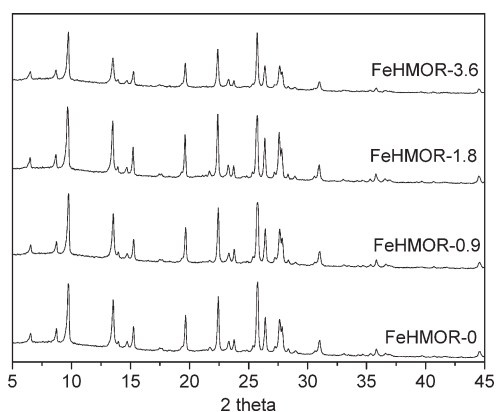


Fig. 1 X-ray diffraction patterns of the FeHMOR samples.

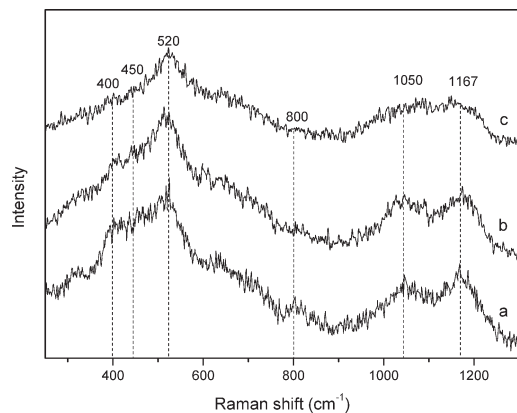


Fig. 2 UV resonance Raman spectra of the FeHMOR samples: a) FeHMOR-0.9, b) FeHMOR-1.8, and c) FeHMOR-3.6.

Raman spectra of Fe-ZSM-5,²⁹ the band at 1165 cm^{-1} is related to the framework crystallinity of the zeolites. The appearance of this band in Fig. 2 for FeHMOR-0.9 and FeHMOR-1.8 indicated that the iron atoms were tightly coordinated in the framework of FeHMOR. However, the remarkable decrease in the intensity of the band for the FeHMOR-3.6 sample illustrated that its crystal state was poor and some iron ions were removed from the framework. Similar results were also observed from the relative crystallinities in Table 1.

The ion exchange of H with Na induced clear modification of the UV-Vis spectra: the appearance of a new peak at about 275 nm and the almost disappearance of the d-d region. These results were confirmed using the UV-Vis spectra of the FeHMOR samples in Fig. 3 and the difference spectrum (FeHMOR – FeNaMOR) in Fig. S4.† According to the literature, the strong charge transfer absorption at about 277 nm represents the Fe^{3+} species in octahedral complexes, and the broad absorption at about 330 nm reveals the presence of octahedral Fe^{3+} present in small clusters, such as that observed for clustered Fe^{3+} in hydroxides.²⁴ As shown in Fig. 3, the decrease of the absorption at 230 nm and increase at 275 nm suggest that the process of ion exchange of H with Na, including ion exchange, drying and calcination, resulted in the removal of some partial tetrahedral Fe^{3+} from the framework and formation of extra-framework octahedral iron species. The peaks in the difference spectra in Fig. S4† indicate that some extra-framework Fe^{3+} species may be in octahedral complexes and some in small clusters. The color of the FeNaMOR zeolites is completely white, indicating the absence of colored oxides of iron in the bulk. But the Fe-containing HMORs were light brown in color, typical of samples containing iron oxides and hydroxides.^{32,33} The diffraction peaks ascribed to iron oxides were not found in the XRD spectra of the four Fe-HMORs after careful comparison and matching. The iron oxides may be highly dispersed in the samples.

The N_2 adsorption curves of all four samples with or without Fe exhibit type I curves (Fig. S5†), the typical N_2 adsorption-desorption isotherms of microporous materials. The corresponding pore volumes and BET surface areas are

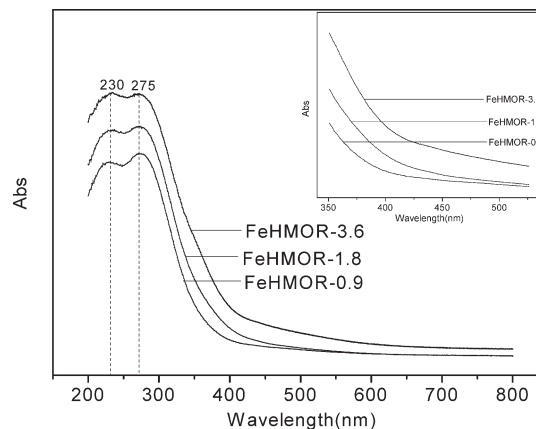


Fig. 3 UV-Vis spectra of the FeHMOR samples.

summarized in Table 2. Comparing the pore volume and micropore volume as well as the BET surface and micropore area, FeHMOR zeolites also proved to be microporous materials. The decrease of nitrogen uptake was observed for the FeHMOR-3.6 sample, which can possibly be attributed to the blocking or filling of micropores by extra-framework species or the low relative crystallinity.

3.2. Catalytic performance

Changes in DME conversion and MAc selectivity with time-on-stream (TOS) for all four catalysts are shown in Fig. 4. The reaction conditions, including the reaction temperature, pressure, gas hourly space velocity and feed composition, were almost the same and thus the obtained DME conversion was indicative of the corresponding catalyst activities in the four tests. The catalytic activities in all experiments initially increased with time and reached maximum values of DME conversion, and then began to decline with further increase in time. Obviously, FeHMOR-0.9 had the highest activity (85%), higher than that of the FeHMOR-0 catalyst (75%), whereas the FeHMOR-3.6 catalyst was the least active (about 40% DME conversion). With the increase of iron content from 0.0 to 3.6%, the maximum value of catalyst activity among the four tests was achieved by FeHMOR-0.9, not by FeHMOR-3.6 or FeHMOR-0. This result is consistent with the changing trend of the BET surface areas and pore volumes, suggesting a close correlation between them in the carbonylation reaction of DME. Detailed research is required to verify the validity of this hypothesis. Also, the corresponding stabilities of all four catalysts exhibited obvious improvement, as shown in Fig. 4b. In addition, the induction periods of all four catalysts were prolonged from 2 to 5 h with the increase of iron content. It was obvious that an appropriate amount of iron in the framework of the mordenite catalysts favored the catalytic performance of DME carbonylation catalysts.

3.3. Analysis of coke retained in deactivated catalysts

The coke in the four deactivated catalysts after DME carbonylation reactions for 12 h at 473 K and 3 MPa was

Table 2 Textural properties of zeolites with different iron contents

	FeHMOR-0	FeHMOR-0.9	FeHMOR-1.8	FeHMOR-3.6
Pore volume ($\text{cm}^3 \text{g}^{-1}$)	0.201	0.210	0.200	0.184
Micropore volume (t -plot, $\text{cm}^3 \text{g}^{-1}$)	0.171	0.177	0.176	0.163
BET surface area ($\text{m}^2 \text{g}^{-1}$)	399	417	403	320
Micropore area (t -plot, $\text{cm}^3 \text{g}^{-1}$)	367	382	377	292

characterized by TG analysis and the results are shown in Fig. 5a and b. All four profiles show two distinct weightlessness peaks in Fig. 5b. The first peak at low temperature can be attributed to the combustion of soft coke (*e.g.* reaction intermediates such as surface bound methyl and acetyl associated with the formation of MAc) and the second peak at high temperature can be assigned to the removal of heavy coke formed during the reaction.^{7,34,35} Fig. 5b shows the combustion temperatures of coke in DTG. It can be observed that the combustion temperatures of heavy coke are significantly different from each other: 843, 803, 748, and 742 K for FeHMOR-0, FeHMOR-0.9, FeHMOR-1.8 and FeHMOR-3.6 respectively, decreasing with increasing iron content of the catalysts. The same trend was obtained for the combustion temperature of soft coke. The difference in

the combustion temperature of hard and soft coke demonstrates that the composition of coke was different in the four samples and the coke molecules became lighter with increasing iron content.

The weight loss of the deactivated FeHMOR-0 catalyst is 10.58 wt%, 81 percent hard coke and 19 percent soft coke. On the other hand, that of the deactivated FeHMOR-1.8 is 10.81 wt% coke with 66% hard coke and 34% soft coke. As the iron amount increased to 3.6 wt%, however, the hard coke and soft coke in the used FeHMOR-3.6 became 45% and 55%, respectively, with a coke amount of 7.02 wt%, much less than that in the used FeHMOR-0 catalyst. Therefore the reactions of coke formation and transformation of soft coke into hard coke were suppressed effectively due to the introduction of iron.

After 12 h of DME carbonylation reaction at 473 K and 3 MPa, the deactivated catalysts were dissolved in HF and

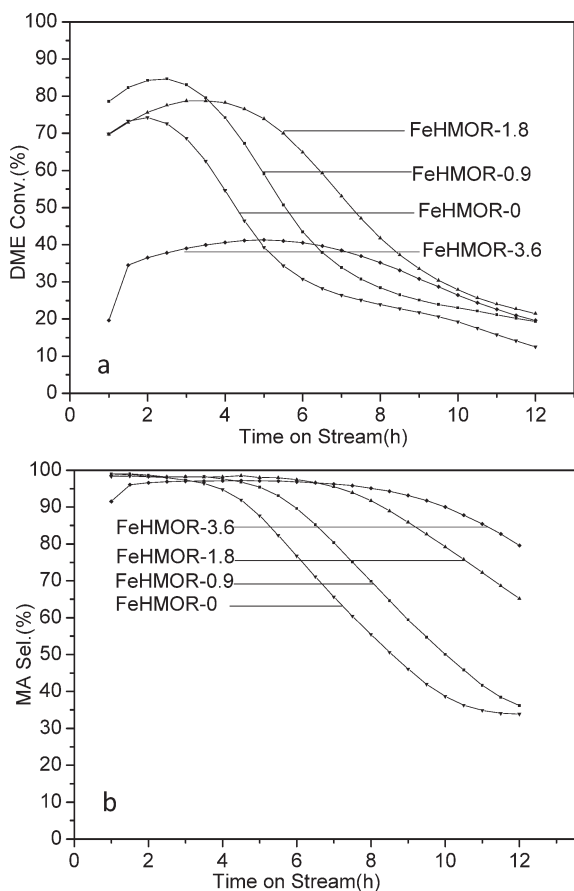


Fig. 4 DME conversion (a) and MAc selectivity (b) of DME carbonylation over Fe-modified HMOR catalysts. Reaction conditions: 473 K, 3.0 MPa, 5%DME, 35%CO, and 60%H₂.

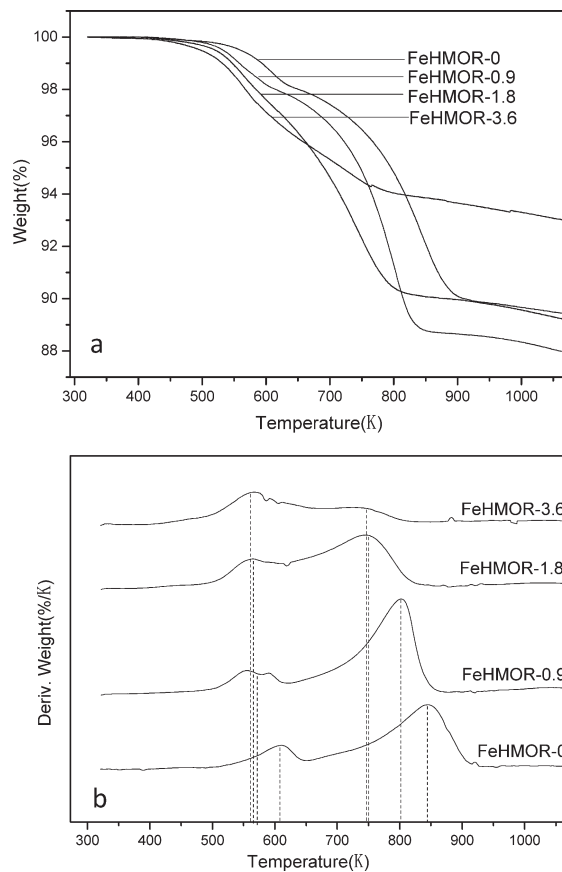


Fig. 5 Thermal analysis of coke in the deactivated catalysts (a: TG; b: DTG).

their chemical compositions are described in detail in Fig. S6.† The structures on the chromatograms are peak identifications made by comparison with the NIST database, and the asterisk (*) represents the internal standard (C_2Cl_6). The adamantane species and methylbenzene species, mainly before the retention time of 25 min, were detected in all spent catalysts. And the species after the retention time of 25 min were mainly bulky polycyclic aromatics. Some higher molecular weight chemical compounds were also detected. The amounts of polycyclic aromatics confined in FeHMOR-0 after 25 min of retention time are obviously more than those in FeHMOR-1.8 and FeHMOR-3.6. The relatively low density of organic species means slight coke deposition during DME conversion, indicating that Fe in the mordenite zeolites can effectively inhibit carbon deposition, which was also confirmed by TG analysis.

As a competitive reaction of DME carbonylation to MAC, DME to olefin reaction forms adamantane species and methylbenzenes species, the important intermediates in the formation of heavy hydrocarbons.³⁶ Accommodation of large hydrocarbon species in the channels of zeolite catalysts greatly limits the mass transfer of reactants and products. When a significant fraction of the 12MR channels of mordenites is occupied by heavy hydrocarbons, catalysts start to deactivate with a decrease in DME conversion and MAC selectivity.

3.4. Characterization of the acid sites in the 12MR channels of mordenite

DME adsorbed on the acid sites in the 12MR channels of mordenite could convert into olefins causing the formation of heavy hydrocarbons through oligomerization and hydride transfer reactions. The intersection of the 12MR channels and 8MR channels would be blocked if the amount of heavy hydrocarbons were enough, which makes the diffusion pathway inefficient for reactants and products.^{7,37} Therefore, removing and/or neutralizing and/or weakening the acid sites in the 12MR channels would be an effective method to improve the stability of MOR catalysts while keeping a high MAC activity.

The T2 and T4 sites in the 12MR channel are the two energetically preferred positions for Fe substitution in the MOR framework, as shown in Fig. S7.†³⁸ The acid sites, with Fe in the framework of the zeolites, are much less active and do not readily catalyze hydride-transfer reactions, thus a much lower tendency to form coke during reactions of olefins is exhibited.³⁹ Therefore, it is supposed that the partial replacement of Al by Fe in the framework would suppress the coke formation reaction to some extent. The information about the concentration and strength of the acid sites in the zeolites would illustrate the current reaction results and the coke composition retained in the catalysts.

FT-IR and solid state NMR spectroscopy techniques have been widely used to characterize the acid sites of zeolites and other solid catalysts by adsorbing basic probe molecules.

The size of TMPO (kinetic diameter *ca.* 0.55 nm) and pyridine (kinetic diameter: 0.585 nm) is slightly smaller than that of the 12-MR channels (0.67 × 0.70 nm) of mordenite, but much larger than that of the 8-MR channels (0.28 × 0.57 nm). TMPO and pyridine would selectively adsorb on the acidic sites located in the 12-MR channels.^{7,40} Therefore ³¹P MAS NMR of adsorbed TMPO has been used to probe surface acidity, as the ³¹P chemical shift of TMPO is sensitive to acid strength.^{41–43} The amount of acid sites in the 12MR channels was characterized by FTIR after adsorption of pyridine.

Fig. S8† displays the ³¹P MAS NMR spectra of the TMPO-adsorbed samples. The signals between 80 and 50 ppm are ascribed to TMPO adsorbed on Brønsted acid sites or chemisorbed species.⁴⁰ The intense signal at 46 ppm is ascribed to physisorbed or weakly adsorbed TMPO. The solid TMPO contributed to the resonance at ~39 ppm.⁴¹ The higher chemical shift of ³¹P reveals stronger acid strength.

All four spectra reveal similar features and can be deconvoluted into three characteristic resonances by Gaussian simulation. The deconvolution results and relative area ratios for the different sites are shown in Table 3.

It is well-known that the higher chemical shift of ³¹P value represents stronger acid strength. Thus acid sites with chemical shifts at site I were identified as strong acid sites, those at site II were moderate acid sites and those at site III weak acid sites. As shown in Table 3, the proportions of strong and moderate acid sites decreased and that of weak acid sites increased correspondingly as the iron content increased from 0.0 to 3.6 wt%. The greater percent of acid sites with lower acid strength would depress the tendency of coke formation. Therefore, the decline of acid strength resulted in the decrease of the amount of coke retained in the catalysts after the introduction of iron atoms.

Pyridine-IR measurements were performed to investigate the acid density mainly in the 12MR channels of mordenite; the results are shown in Fig. 6. In general, the two adsorption peaks at ~1450 and 1540 cm^{-1} correspond to the characteristic vibration peaks of pyridine molecules adsorbed on Lewis and Brønsted acid sites, forming PyL (pyridine bonded to Lewis sites) and Py⁺ (pyridinium ions), respectively.⁴⁴ The adsorption peak at around 1490 is usually classified as Brønsted and Lewis acid sites.

The concentrations of Brønsted and Lewis acid sites in the FeHMOR samples were calculated from the IA area of the bands at about 1540 and 1450 cm^{-1} according to the extinction coefficients reported by Emeis.²¹ The calculation results are shown in Fig. 7. The concentration of acid sites which

Table 3 Distributions of Brønsted acid sites on various catalysts as detected by ³¹P MAS NMR using TMPO as a probe molecule

	Site I ~82 ppm area (%)	Site II ~67 ppm area (%)	Site III ~51 ppm area (%)
FeHMOR-0	4.81	39.99	55.20
FeHMOR-0.9	4.65	42.39	52.96
FeHMOR-1.8	1.93	36.37	61.71
FeHMOR-3.6	1.98	35.13	62.89

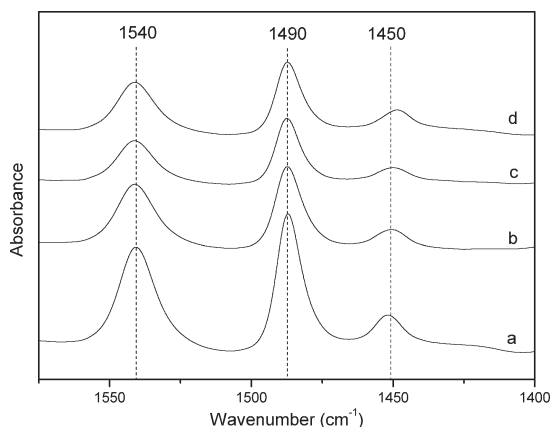


Fig. 6 Pyridine-IR spectra of the FeHMOR samples: a) FeHMOR-0; b) FeHMOR-0.9; c) FeHMOR-1.8; and d) FeHMOR-3.6.

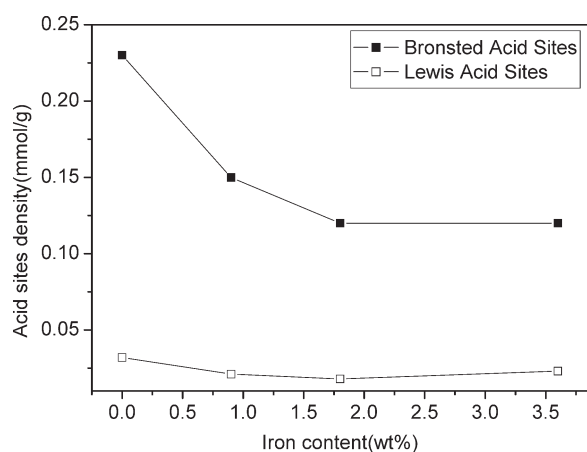


Fig. 7 The quantitative calculation of Brønsted and Lewis acid sites mainly in the 12MR channels of mordenite.

would adsorb pyridine molecules at 573 K decreased from 0.23 to 0.12 mmol g⁻¹ when the iron content increased from 0.0 to 3.6 wt%. As a consequence, the oligomerization and hydride reactions leading to the formation of coke were effectively suppressed,³⁹ which can be demonstrated by the decrease of the coke amount and the combustion temperature with the increase of iron content in the catalysts (shown in Fig. 5). Therefore, the stability of the FeHMOR catalysts during the tests for DME carbonylation improved, as shown in Fig. 4b.

Conclusions

In this study, a series of mordenite samples with varying iron contents from 0.0 to 3.6 wt% in zeolites were synthesized by a template-free method and employed in DME carbonylation reaction. Fe atoms were introduced into the framework of mordenite zeolite and the acid strength and density in the 12MR channels of mordenite were found to be reduced after the introduction of Fe in the zeolite framework, as evidenced by the characterization results of ³¹P MAS NMR and FTIR. As

a consequence, the performance of the FeHMOR samples was markedly improved. With the increase of iron content from 0.0 to 3.6 wt%, DME conversion increased and then decreased. Also, the corresponding stabilities of all four catalysts continued to increase. These results are due to the inhibition of coke formation in the 12MR channels of mordenite during DME carbonylation reaction. The corresponding amount of coke in the used catalysts was reduced with the increase of iron content. And the deposited chemical compounds on the catalysts were primarily adamantane species, methylbenzenes and polycyclic aromatics. The results obtained in this study with iron modified mordenite catalysts are encouraging, and further studies on the improvement of their performance are required.

Acknowledgements

We acknowledge the financial support from the National Natural Science Foundation of China (grant no. 21473182 and 21303106).

Notes and references

- 1 K. Fujimoto, T. Shikada, K. Omata and H. Tominaga, *Chem. Lett.*, 1984, 2047–2050.
- 2 A. Bhan, A. D. Allian, G. J. Sunley, D. J. Law and E. Iglesia, *J. Am. Chem. Soc.*, 2007, **129**, 4919–4924.
- 3 P. Cheung, A. Bhan, G. J. Sunley and E. Iglesia, *Angew. Chem., Int. Ed.*, 2006, **45**, 1617–1620.
- 4 P. Cheung, A. Bhan, G. Sunley, D. Law and E. Iglesia, *J. Catal.*, 2007, **245**, 110–123.
- 5 M. Boronat, C. Martinez-Sanchez, D. Law and A. Corma, *J. Am. Chem. Soc.*, 2008, **130**, 16316–16323.
- 6 B. Li, J. Xu, B. Han, X. Wang, G. Qi, Z. Zhang, C. Wang and F. Deng, *J. Phys. Chem. C*, 2013, **117**, 5840–5847.
- 7 J. Liu, H. Xue, X. Huang, P. Wu, S. Huang, S. Liu and W. Shen, *Chin. J. Catal.*, 2010, **31**, 729–738.
- 8 H. Xue, X. Huang, E. Zhan, M. Ma and W. Shen, *Catal. Commun.*, 2013, **37**, 75–79.
- 9 M. D. Jones, C. G. Keir, C. D. Iulio, R. A. M. Robertson, C. V. Williams and D. C. Apperley, *Catal. Sci. Technol.*, 2011, **1**, 267–272.
- 10 R. N. Singh and R. Awasthi, *Catal. Sci. Technol.*, 2011, **1**, 778–783.
- 11 R. K. Niven, *Renewable Sustainable Energy Rev.*, 2005, **9**, 535–555.
- 12 P. D. Vaidya and A. E. Rodrigues, *Chem. Eng. J.*, 2006, **117**, 39–49.
- 13 A. C. Hansen, Q. Zhang and P. W. Lyne, *Bioresour. Technol.*, 2005, **96**, 277–285.
- 14 X. G. San, Y. Zhang, W. J. Shen and N. Tsubaki, *Energy Fuels*, 2009, **23**, 2843–2844.
- 15 M. Hartmann and L. Kevan, *Chem. Rev.*, 1999, **99**, 635–664.
- 16 B. Ellis, M. J. Howard, R. W. Joyner, K. N. Reddy, M. B. Padley and W. J. Smith, *11th International Congress on Catalysis - 40th Anniversary, Pts a and B*, 1996, vol. 101, pp. 771–779.

- 17 T. Blasco, M. Boronat, P. Concepcion, A. Corma, D. Law and J. A. Vidal-Moya, *Angew. Chem., Int. Ed.*, 2007, **46**, 3938–3941.
- 18 X. Zhang, Y. P. Li, S. B. Qiu, T. J. Wang, M. Y. Ding, Q. Zhang, L. L. Ma and Y. X. Yu, *Chin. J. Chem. Phys.*, 2013, **26**, 77–82.
- 19 V. I. Sobolev, G. I. Panov, A. S. Kharitonov, V. N. Romannikov, A. M. Volodin and K. G. Ione, *J. Catal.*, 1993, **139**, 435–443.
- 20 M. A. Uddin, T. Komatsu and T. Yashima, *J. Catal.*, 1994, **150**, 439–441.
- 21 C. A. Emeis, *J. Catal.*, 1993, **141**, 347–354.
- 22 M. Guisnet, L. Costa and F. R. Ribeiro, *J. Mol. Catal. A: Chem.*, 2009, **305**, 69–83.
- 23 P. Wu, T. Komatsu and T. Yashima, *Microporous Mesoporous Mater.*, 1998, **20**, 139–147.
- 24 S. Bordiga, R. Buzzoni, F. Geobaldo, C. Lamberti, E. Giamello, A. Zecchina, G. Leofanti, G. Petrini, G. Tozzola and G. Vlaic, *J. Catal.*, 1996, **158**, 486–501.
- 25 T. Inui, H. Nagata, T. Takeguchi, S. Iwamoto, H. Matsuda and M. Inoue, *J. Catal.*, 1993, **139**, 482–489.
- 26 P. Ratnasamy and R. Kumar, *Catal. Today*, 1991, **9**, 329–416.
- 27 C. Li, G. Xiong, J. Liu, P. Ying, Q. Xin and Z. Feng, *J. Phys. Chem. B*, 2001, **105**, 2993–2997.
- 28 K. Sun, F. Fan, H. Xia, Z. Feng, W.-X. Li and C. Li, *J. Phys. Chem. C*, 2008, **112**, 16036–16041.
- 29 F. Fan, K. Sun, Z. Feng, H. Xia, B. Han, Y. Lian, P. Ying and C. Li, *Chem. – Eur. J.*, 2009, **15**, 3268–3276.
- 30 J. Wang, H. Xia, X. Ju, F. Fan, Z. Feng and C. Li, *Chin. J. Catal.*, 2013, **34**, 876–888.
- 31 H. Xin, J. Liu, F. Fan, Z. Feng, G. Jia, Q. Yang and C. Li, *Microporous Mesoporous Mater.*, 2008, **113**, 231–239.
- 32 A. Meagher, V. Nair and R. Szostak, *Zeolites*, 1988, **8**, 3–11.
- 33 J. Perez-Ramirez, F. Kapteijn and A. Bruckner, *J. Catal.*, 2003, **218**, 234–238.
- 34 M. Guisnet and P. Magnoux, *Appl. Catal., A*, 2001, **212**, 83–96.
- 35 L. Palumbo, F. Bonino, P. Beato, M. Bjorgen, A. Zecchina and S. Bordiga, *J. Phys. Chem. C*, 2008, **112**, 9710–9716.
- 36 H. Xue, X. Huang, E. Ditzel, E. Zhan, M. Ma and W. Shen, *Ind. Eng. Chem. Res.*, 2013, **52**, 11510–11515.
- 37 B. Li, J. Xu, B. Han, X. Wang, G. Qi, Z. Zhang, C. Wang and F. Deng, *J. Phys. Chem. C*, 2013, **117**, 5840–5847.
- 38 S. P. Yuan, J. G. Wang, Y. W. Lia and H. J. Jiao, *J. Mol. Struct.: THEOCHEM*, 2004, **674**, 267–274.
- 39 O. Kresnawahjuesa, *J. Catal.*, 2002, **210**, 106–115.
- 40 A. Zheng, B. Han, B. Li, S. B. Liu and F. Deng, *Chem. Commun.*, 2012, **48**, 6936–6938.
- 41 S. Hayashi and N. Kojima, *Microporous Mesoporous Mater.*, 2011, **141**, 49–55.
- 42 A. Zheng, H. Zhang, X. Lu, S. B. Liu and F. Deng, *J. Phys. Chem. B*, 2008, **112**, 4496–4505.
- 43 A. Zheng, S. J. Huang, S. B. Liu and F. Deng, *Phys. Chem. Chem. Phys.*, 2011, **13**, 14889–14901.
- 44 P. Ayrault, J. Datka, S. Laforge, D. Martin and M. Guisnet, *J. Phys. Chem. B*, 2004, **108**, 13755–13763.